Dynamic Performance Optimization of Monorail Rapid Transit Formation Vehicles Based on Improved Artificial Potential Field Algorithm

Haoxin WU*, Zixue DU**, Zhen YANG***, Xiaoxia WEN****

*Institute of Urban Rail, Chongqing Jiaotong University, 400074 Chongqing, P.R. China, E-mail:15310165464@163.com
**Institute of Urban Rail, Chongqing Jiaotong University, 400074 Chongqing, P.R. China, E-mail: aaadzx@163.com
(Corresponding author)
***Institute of Urban Rail, Chongqing Jiaotong University, 400074 Chongqing, P.R. China, E-mail: 21930315@qq.com
****Institute of Urban Rail, Chongqing Jiaotong University, 400074 Chongqing, P.R. China,
E-mail: 963884811@qq.com

1. Introduction

The expensive construction and operation costs of subway lines have become a huge financial burden for local governments. In order to prevent excessive local fiscal deficits, China has issued a series of policies to restrict the construction of subway lines. At present, this restriction is gradually strengthened. Some large and medium-sized cities with urban rail transit construction needs are unable to build their own urban rail transit lines due to policy and financial constraints. In this context, the urban rail transit industry is exploring new solutions, and many companies have developed new urban rail transit systems, such as Automated People Mover System (APM), straddle monorail system, suspended monorail system, etc. However, the construction and operation costs of these urban rail transit systems are too expensive for many medium-sized cities with great financial pressure in China. Therefore, it is still necessary to design a new urban rail transit system to meet the needs of the city. In this case, in order to meet the huge urban rail transit construction market with medium and low traffic volume in the future, this team proposed a small monorail rapid transit system [1-2].

The core concepts of the planning and design of the new monorail rapid transit system are miniaturization, unmanned and networking. Miniaturization refers to the miniaturization of vehicles and stations, which is mainly to reduce the purchase cost of vehicles and the huge construction cost of stations. Unmanned refers to driverless and unattended stations, mainly to reduce the huge labor costs of the operating company for employees. Networking refers to the network operation of the line, which can improve the service level and increase the probability of residents choosing it as a travel mode. These ideas are mainly to design a low cost and medium volume rail transit system suitable for medium-sized urban trunk lines, large urban feeder lines or tourist lines.

In addition, the system adopts virtual coupling technology. It can flexibly adjust the line capacity according to the real-time business requirements to minimize the operation and maintenance costs. However, for the existing urban rail transit system, it is difficult to transform and apply virtual coupling. It can be seen that the new monorail rapid transit system can solve many problems of the existing urban rail transit. In related fields, many experts and scholars have begun to study some key technologies.

In the field of straddle monorail system, many vehicles with mature technology have been put into operation, and the current research is still focused on single axle [3] and double axle straddle monorail. Relevant research focuses on vehicle dynamics analysis [4] and tire wear analysis [5]. They mainly use finite element method (FEM) and dynamic simulation methods to optimize the vehicle structure, suspension and tire parameters, but lack of innovative design of vehicle structure.

In the field of virtual coupling of rail vehicles, many scholars mainly study the control algorithm of formation vehicles, such as model predictive control algorithm [6-7], optimal control [8-9], reinforcement learning [10], etc. The research objects are all steel wheel and rail systems, such as the "European shift2rail project" [11]. However, for high-speed and city railways, due to the large curve radius of the line and the long distance between vehicles, the dynamic problems caused by the different curve radius of each vehicle when the formation of vehicles passes through the curve were not considered in the study. For the new type of monorail rapid transit system, the vehicle dynamics problems caused by the formation vehicles passing through the small radius curve with small formation spacing have to be considered. Therefore, it is necessary to establish the vehicle dynamics model and multi-body dynamics simulation model for the special structure of the new type of monorail rapid transit vehicle, and optimize the dynamic performance of the formation passing through the small radius curve.

This paper first briefly introduces the new monorail rapid transit system proposed by the team, analyzes its vehicle structure, and establishes the vehicle dynamics model and multi-body dynamics simulation model. Then, based on the improved artificial potential field (APF) algorithm, the formation vehicle operation controller is established, and the evaluation index is constructed. Finally, the dynamic performance of the formation vehicle passing through the small radius curve is optimized.

2. Structural analysis of vehicle

In terms of structure, the new type of monorail rapid transit vehicle is different from the traditional straddle monorail vehicle. Fig. 1 and Fig. 2 show Chongqing straddle monorail line 3 and the new type of monorail rapid transit vehicle respectively. In Fig. 1, a vehicle has two bogies.

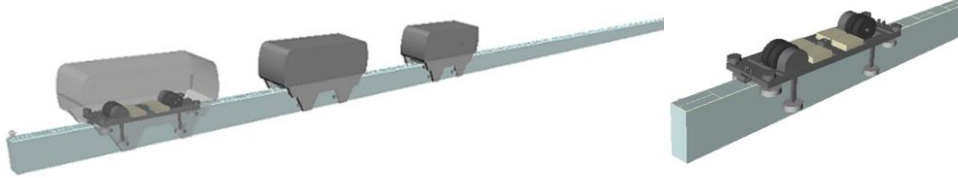Fig. 1 Chongqing straddle monorail line 3 and its bogie

Fig. 2 New type monorail rapid transit vehicle and its bogie

Each bogie has four running wheels, four steering wheels and two stabilizing wheels. The traction energy of the vehicle is provided by the substation beside the line, and the electric energy is transmitted to the power system by the pantograph on the bogie. In Fig. 2, a vehicle has only one bogie, with a total of 4 running wheels, 4 steering wheels and 4 stabilizing wheels, and its power supply is provided by power battery.

It can be seen from Fig. 1 and 2 that the structure of the new monorail rapid transit vehicle is very different from that of the traditional straddle monorail vehicle. First, the miniaturization of vehicles reduces the cost of vehicle purchase, with smaller curve radius and more flexible route selection. Secondly, the vehicle is driven by power battery, which avoids the construction cost of pantograph catenary power supply system and eliminates the noise of pantograph catenary contact. Moreover, due to the lack of physical couplers on vehicles, the line can be set with a larger slope.

Table 1 shows the design parameters of these two systems. It can be seen that the structure of the new type of monorail rapid transit vehicle is quite different from that of the traditional straddle monorail vehicle. In the dynamic modeling, it is necessary to conduct a specific analysis according to the characteristics of its structure.

3. Vehicle dynamic model

The dynamic model of the new monorail rapid transit vehicle is shown in Fig. 3. It can be seen that the number and arrangement of wheels are different from the traditional bogie. The longer wheelbase of running wheel brings better anti pitching ability. The secondary suspension adopts the combination of bag type air spring and rubber stop device, which can effectively alleviate vehicle vibration. In addition, the low floor design can not only effectively reduce the vehicle centroid and improve the vehicle stability, but also reduce the cross-sectional area occupied by the vehicle and reduce the tunnel excavation area.

The vertical and lateral movement of bogie can be expressed as:

$$M_b \ddot{Z}_b + 4k_{2z}\left(Z_b - Z_f\right) + 4c_{2z}\left(\dot{Z}_b - \dot{Z}_f\right) = F_z , \tag{1}$$

$$M_b \ddot{Y}_b + 4k_{2y}\left(Y_b - Y_f - \varphi_f l_{fz} + \varphi_b l_{bz}\right) +$$
$$+ 4c_{2y}\left(\dot{Y}_b - \dot{Y}_f - \dot{\varphi}_f l_{fz} + \dot{\varphi}_b l_{bz}\right) = F_y , \tag{2}$$

Table 1

Main parameters of vehicle

|	Chongqing straddle monorail line 3	New type monorail rapid transit vehicle
Number of running wheels	8	4
Number of steering wheels	8	4
Number of stabilizing wheels	4	4
Vehicle length	14.8 m(Mc), 13.9 m(M)	7 m
Unloaded mass	28.6 t(Mc), 27.6 t(M)	8 t
Minimum curve radius (main line)	100 m	50 m
Maximum speed	80 km/h	80 km/h
Maximum slope (main line)	60‰	12‰
Power supply mode	Pantograph and catenary	Power battery
Vehicle formation mode	Fixed group	Virtual coupling
Line construction cost	0.3~0.5 billion RMB (/km)	<0.1 billion RMB (/km)
Freight volume	10000~30000 passengers per hour	3000~15000 passengers per hour
Station length	>120 m	11m (only parking 1 vehicle) 40 m (Maximum parking 4 vehicles) 76 m (Maximum parking 8 vehicles)
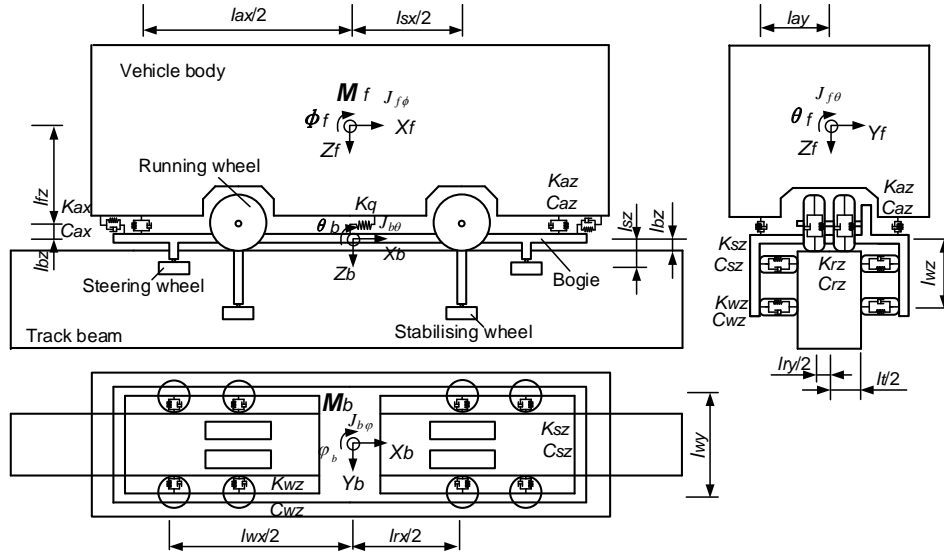
Fig. 3 Dynamic model of new type monorail rapid transit vehicle

where F_y and F_z are the transverse and vertical excitation of the track acting on the bogie respectively; M_f is the mass of the vehicle body; M_b is the mass of bogie; K_{az} and C_{az} are the vertical stiffness and damping of the secondary suspension; l_{fz} and l_{bz} are the height from the center of gravity of the vehicle to the secondary suspension and the height from the secondary suspension to the center of gravity of the bogie, respectively.

Based on the dynamic model of the vehicle, the multi-body dynamics simulation model of the vehicle is established in SIMPACK, as shown in Fig. 4. The simulation model is a multi-rigid body dynamic model. Except for the tire and suspension force element, the deformation of each component is ignored in modeling. F-tire model is used for tire modeling, and its data is added to SIMPACK by reading tire files.
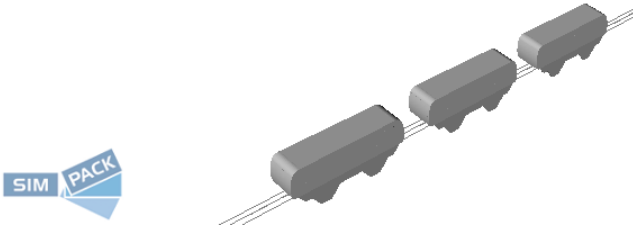

Fig. 4 Multi-body dynamics simulation model

Table 2

Vehicle parameters

Parameters	Values	Unit
Vehicle body mass	3000	kg
Bogie mass	5000	kg
Wheelbase of running wheel axle	3.5	m
Longitudinal spacing of steering wheel	5.2	m
Longitudinal spacing of stabilizing wheel	4.3	m
Height of steering wheel from rail surface	0.34	m
Height of stabilizing wheel from rail surface	0.83	m
Vertical stiffness of air spring	150000	N/m
Air spring vertical damping	15000	Ns/m
Preload of steering wheel	5200	N
Preload of stabilizing wheel	3000	N

The modeling method of Chongqing straddle type monorail line 3 is adopted for the modeling of running road. The irregularity data is imported into SIMPACK for fitting to simulate the irregularity of track surface. According to laser scanning analysis and vehicle dynamic testing, the running surface roughness is similar to the A-level specified in ISO 8606: 2016, so the running surface roughness in the model is A-level road surface [12]. Some parameters of the vehicle multi body dynamics simulation model are shown in Table 2.

4. Formation vehicle operation controller

4.1. Vehicle longitudinal dynamics model

The vehicle longitudinal dynamics model adopts the same calculation method as in [1]. The calculation method of vehicle running resistance can be expressed as:

$$\sum F = F_f + F_w + F_s + F_r + F_a + F_t, \qquad (3)$$

where F_f is the rolling resistance of the vehicle, F_w is the air resistance of the vehicle, F_s is the ramp resistance, F_r is the curve resistance of the vehicle passing through the curve, F_a is the acceleration resistance, F_t is the tunnel resistance.

The traction force u required by the vehicle is:

$$u = Ma + \sum F, \qquad (4)$$

where a and M are vehicle acceleration and vehicle mass respectively.

4.2. Improved artificial potential field algorithm

The artificial potential field algorithm constructs the surrounding of the obstacle as a repulsive potential field, and the surrounding of the target point as a gravitational potential field. When the vehicle is moving, it calculates the potential field force it receives to move towards the target point, and bypasses the obstacle at the same time. During the longitudinal formation movement of rail vehicles, the lateral obstacle avoidance of vehicles is realized through

switches and signal systems due to the longitudinal movement of vehicles along the fixed track. Therefore, we will improve the traditional artificial potential field algorithm to make it more suitable for the formation of rail transit vehicles.

The required traction force of the vehicle can be expressed as:

$$u = k_1 \tanh\left(x_i - x_j - d_{ij}\right) + k_2 \tanh\left(v_i - v_j\right), \qquad (5)$$

where k_1 and k_2 are the control gain coefficients of displacement and velocity, x_i and x_j are the positions of the front and rear vehicles, v_i and v_j are the speeds of the front and rear vehicles, and d_{ij} is the desired distance between the front and rear vehicles, d_{ij} can be expressed as:

$$d_{ij} = d_{stop} + v_j t_s, \qquad (6)$$

where d_{stop} is the parking distance of formation vehicles.

In existing research, the targets considered for the formation movement of rail transit vehicles include positions and speeds approaching the target values, as shown in Eq. (7). It did not take into account the impact of the different positions of each vehicle on the formation of vehicles passing through small curve radius.

$$\begin{cases} \lim\limits_{t \to t_k}\left(x_i - x_j\right) = d_{ij} \\ \lim\limits_{t \to t_k}\left(v_i - v_j\right) = 0 \end{cases}, \qquad (7)$$

where t_k is the maximum convergence time of formation stable operation. If t_k is too large, the formation cannot converge in a short time, which affects the efficiency of line operation.

According to the control objective of Eq. (7), if the dynamic performance of each vehicle is not considered when the formation vehicle moves on the small radius curve line, it will inevitably affect the safety and comfort of each vehicle. Therefore, the control quantity of speed when the vehicle passes through the curve is added in Eq. (5), so that it can adjust the traction force in real time according to the curvature of the line.

$$u = k_1 \tanh\left(x_i - x_j - d_{ij}\right) + k_2 \tanh\left(v_i - v_j\right) + \\ + k_3 \tanh\left(v_j - v_j^*\right), \qquad (8)$$

where v_j^* is the relative optimal speed of vehicle j passing through the curve.

Through this control method, the speed of the vehicle on the curve can approach the speed with relatively optimal dynamics. The speed is related to the superelevation and curve radius of the line, and can be calculated briefly according to Eq. (9).

$$v_j^* = \sqrt{12.96 * hRg}, \qquad (9)$$

where h is the actual superelevation of the line, which is taken as 12% in this paper.

In addition, the values of k_1, k_2 and k_3 in Eq. (8) affect the control of formation vehicles. They represent the control degree of spacing, speed, and dynamics through the curve. In order to ensure the optimal dynamic performance of the vehicle when passing through the curve, k_1 and k_2 can be set as small values and k_3 as large values. This can weaken the control effect of formation when the vehicle passes through the curve, and give priority to meeting its own dynamic performance. If k_1, k_2 and k_3 are equal, the formation control effect is still guaranteed when crossing the curve. In order to ensure the priority of dynamic performance, the control parameter is set as $k_3 = 2k_1 = 2k_2$ when the vehicle passes the curve.

Furthermore, the distance between vehicles in formation must be greater than the minimum safety protection distance. Considering the limitations of vehicle acceleration and braking performance, the controller also needs to restrict the acceleration of each vehicle, as shown in Eq. (10).

$$a_{tmax} < a_j < a_{bmax}, \qquad (10)$$

where a_{tmax} and a_{bmax} are the maximum acceleration and maximum deceleration of the vehicle during normal operation, respectively.

5. Vehicle dynamics evaluation index

When the formation vehicles pass through the curve, it is necessary to ensure that the dynamic performance of each vehicle in the formation meets the requirements of running stability, ride comfort and curve passing ability.

5.1. Running stability

Generally, overturning coefficient is mainly used to evaluate the running stability of vehicles, which can be expressed as:

$$D = \frac{\Delta P}{P} = \frac{P_2 - P_1}{P_2 + P_1}, \qquad (11)$$

where P_1 is the vertical force of the wheel at the load reduction side; P_2 is the vertical force of the wheel on the load increase side.

This index is widely used in rail transit vehicles with steel wheel-rail vehicle, and the value must not be greater than 0.8. However, the running mechanism and dynamic performance of monorail vehicles with rubber tires are different from the former, so new evaluation index is needed to evaluate their running stability. Therefore, we propose the index of load transfer coefficient of running wheels to evaluate the running stability of vehicles, which can be expressed as:

$$C_{rt} = \frac{P_z - P_j}{P_0}, \qquad (12)$$

where P_z is the radial load of the running wheel on the load increase side; P_j is the radial load of the running wheel on the load shedding side; P_0 is the radial load of the running wheel axle.

In addition, when the vehicle is about to lose stability due to a large overturn, the vehicle is also in a relatively safe state due to the existence of steering wheels and

stabilizing wheels. Therefore, we have established an evaluation system for the load transfer coefficient of running wheels, as shown in Table 3.

Table 3

Evaluation level of C_{rt}

C_{rt}	Evaluation level
0~0.6	Good
0.6~0.7	Average
0.7~0.9	Pass
>0.9	Poor

5.2. Ride comfort

When the vehicle passes through the curve, the unbalanced centrifugal acceleration is generally used to evaluate its comfort. The evaluation grade of unbalanced centrifugal acceleration has different standards in different regions according to the experimental lines and vehicle systems [13], as shown in Table 4. Many factors will make passengers give different evaluations, such as vehicle system, center of gravity and maximum speed. For another example, because the body of a suspended monorail vehicle is in the air, the passengers' bearing capacity to the unbalanced centrifugal acceleration will certainly be weakened. Therefore, we need to select the evaluation level suitable for the new monorail rapid transit to evaluate the unbalanced centrifugal acceleration.

Table 4

Unbalanced centrifugal acceleration (a_y) test results of various regions

Area	Scope of evaluation index (m/s^2)
Britain and America	0.4~1.0 is an allowed value
Japan	<0.78
Hungary	0.33~0.65
Germany	<0.65, have no adverse reactions
France and Italy	<0.85, do not feel uncomfortable
International Union of Railways (UIC)	<1.16, most passengers do not feel uncomfortable
China	<0.4, have a slight sensation; >0.8, clearly uncomfortable

In general, measured values are greater than theoretical calculations, with coefficients ranging from 1.2 to 1.3. The test evaluation levels vary in different regions, but the limit values that passengers can withstand are generally within the range of 0.3 to 1.2 m/s^2, with the range of 0.4 to 0.8 m/s^2 being the main range. Therefore, this article adopts the widely used acceleration range as the evaluation level, which is shown in Table 5.

Table 5

Evaluation level of a_y

a_y	Passenger's feelings	Evaluation level
< 0.4	No obvious sensation	Good
< 0.5	Able to perceive, but without uncomfortable feelings	Average
< 0.8	Ordinary passengers can withstand it for a long time	Pass

5.3. Curve passing ability

The roll attitude of the vehicle body when passing through the curve reflects the ability of the vehicle to pass through the curve. This article uses the roll angle of the vehicle body to evaluate the curve passing ability of the vehicle, and its evaluation level is shown in Table 6.

Table 6

Evaluation level of vehicle body roll angle

Vehicle body roll angle (°)	Evaluation level
<3	Good
3~5	Average
5~6	Pass

Moreover, the distance between vehicles should meet their own safety protection needs to avoid collisions.

$$S_{vij} < S_{vminij}, \qquad (13)$$

where S_{vij} and S_{vminij} are the driving distance and the minimum driving distance of adjacent vehicles, respectively.

6. Simulation and Analysis

6.1. Simulation scenario

In order to compare the control effectiveness of the controller, the pilot vehicle was operated using the set speed curve during simulation, and the designed formation controller was used to control the following vehicle. Using a pilot vehicle to simulate the situation where a vehicle passes through a curve without dynamic control, and comparing it with two following vehicles with dynamic control. This section uses three vehicle formations for simulation, with a line curve radius of 50 meters.

6.2. Simulation results and analysis

The speed change curve and relative position change curve of the three-vehicle formation passing through the line with a radius of 50 meters are shown in Fig. 5 and 6, respectively.

As can be seen from Fig. 5 and 6, when the formation enters the transition curve at 13s, the speed of the following vehicles decreases rapidly, and the distance between vehicles also increases accordingly. On the transition curve, following vehicles weakens the control effect of the formation and enhances the control effect on its own dynamic performance. When passing through a circular curve, the speed of the following vehicle decreases to the calculated relative optimal speed. After the vehicle left the curved line, the controller immediately restored control of the formation effect. The control target immediately becomes to control over vehicle speed and spacing. At 55s, the following vehicle and the pilot vehicle reached a stable speed and relative distance.

It can be seen that the improved artificial potential field controller can flexibly adjust the vehicle speed when passing through the curve, and can also restore the control effect on the formation after the vehicle leaves the curve line.

The radial force of the running wheels of the formation vehicles is shown in Fig. 7, which shows the change in force on the running wheels when the vehicle passes through the curve. V1, V2, and V3 represent the leading vehicles and two following vehicles in the formation, FF and FR represent the running wheels on the left and right sides
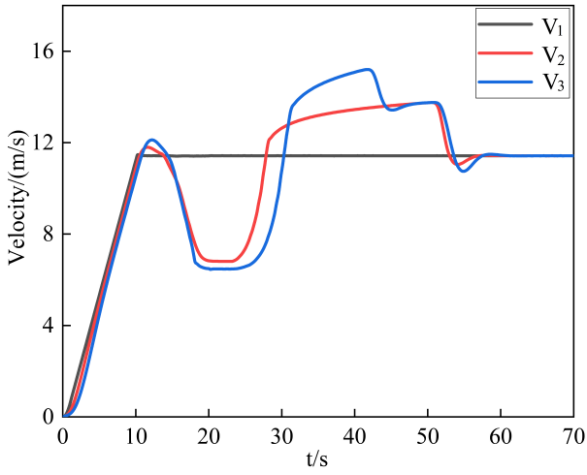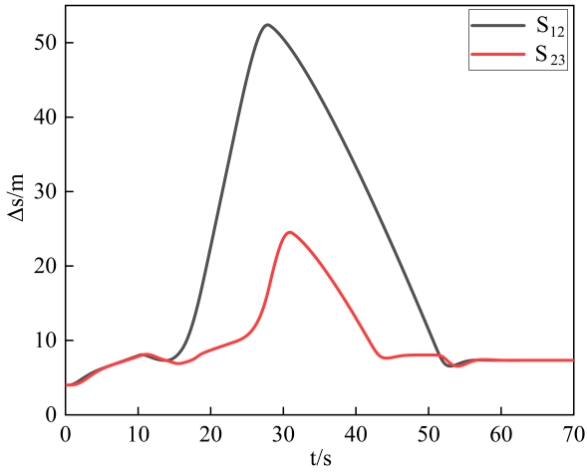
Fig. 5 Speed curve of formation vehicles

Fig. 6 Longitudinal position difference between adjacent vehicles

of the front axle on each vehicle's bogie, RL and RR represent the running wheels on the left and right sides of the rear axle, respectively.

According to the calculation Eq. (12) of C_{rt}, use the data in Fig. 7 to calculate the C_{rt} variation curve for each vehicle, as shown in Fig. 8. In Fig. 8, V1F and V1R represents the front and rear axles of the pilot vehicle, respectively.

It can be seen from Fig. 7 and 8 that C_{rt} of the pilot vehicle is much larger than that of the follower vehicle when passing through the curve. Because the pilot vehicle did not control its dynamic performance, its C_{rt} maximum reached 0.39. Due to the control of dynamics, the following vehicle has a certain deceleration behavior when passing through the curve, so its C_{rt} is significantly lower than that of the pilot vehicle. The maximum C_{rt} values of the two following vehicles were 0.174 and 0.14 respectively, which were far lower than the index requirements. By comparing the amplitude of C_{rt} curve when the pilot vehicle and the follower vehicle pass through the curve, it can be clearly seen that the improved artificial potential field controller has the optimization effect on the operation stability of formation vehicles.

The unbalanced centrifugal acceleration of formation vehicles is shown in Fig. 9. It can be seen from Fig. 9 that before the formation enters the transition curve, a_y is almost zero, and the curve fluctuates after each vehicle enters the transition curve. The maximum a_y of the pilot vehicle exceeds 0.4 m/s^2 and reaches 0.433 m/s^2. According to the evaluation index, its ride comfort is average. The maximum values of the following vehicles are 0.055 m/s^2 and 0.053 m/s^2 respective ly, which are far lower than 0.4 m/s^2. By comparing a_y of the pilot vehicle and the follower vehicle when they pass through the curve, it can be seen that the improved artificial potential field controller has an optimal effect on the ride comfort of formation vehicles. The roll angle of formation vehicles is shown in Fig. 10.
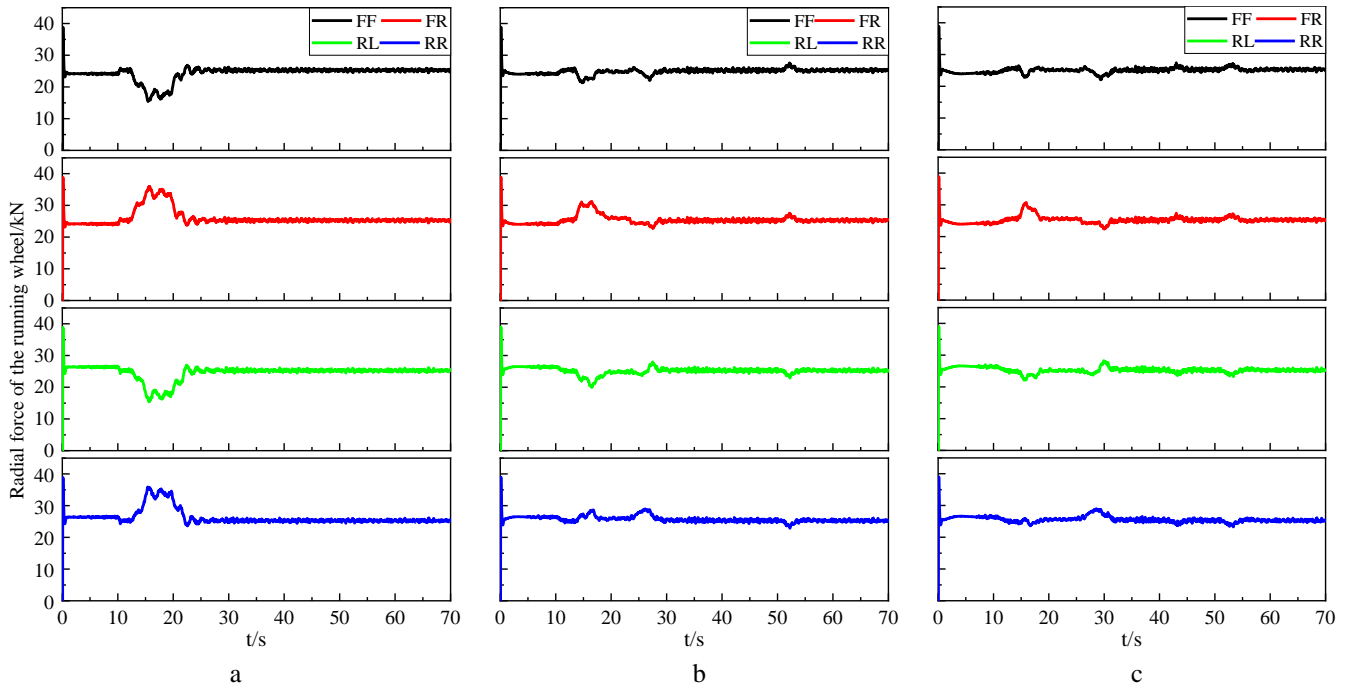

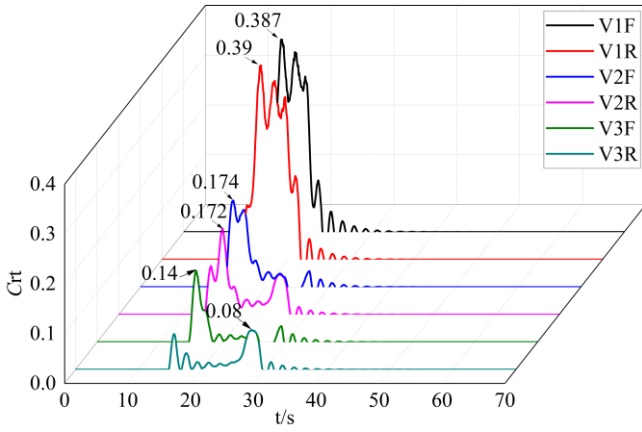Fig. 7 Radial force of running wheels of formation vehicles: a – V1, b – V2, c – V3

Fig. 8 Load transfer coefficient of running wheels of formation vehicles
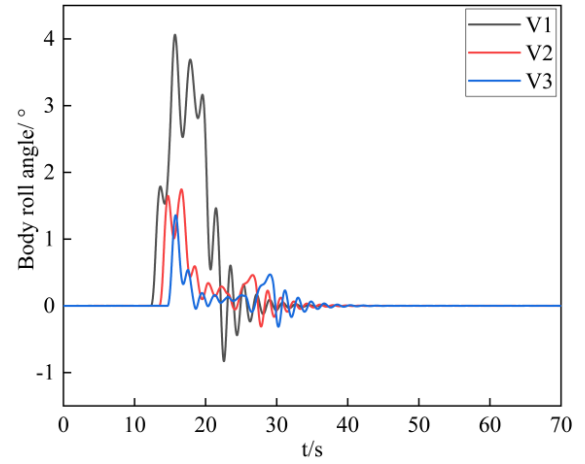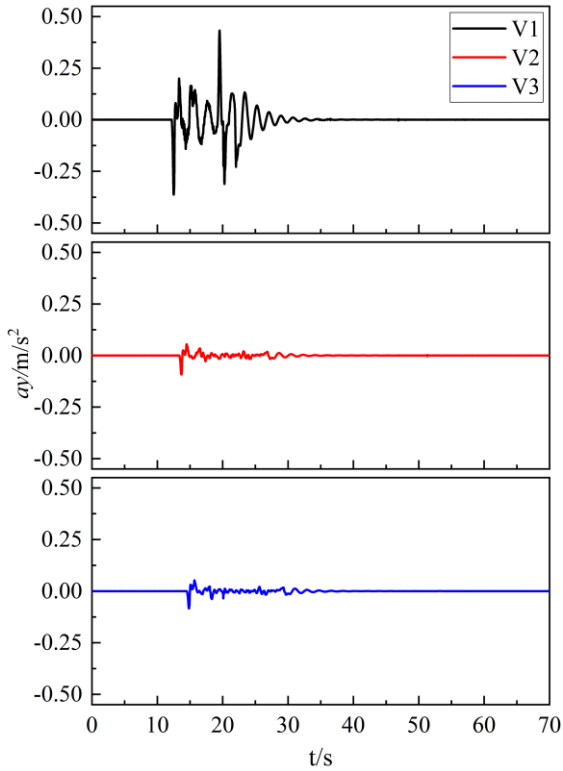

Fig. 10 Roll angle of formation vehicle

Fig. 9 Unbalanced centrifugal acceleration of formation vehicles

Table 7
Summary of simulation results data

Evaluation index	Vehicle	Result	Evaluation level
Crt	V1	0.39	Good (<0.6)
	V2	0.174	Good (<0.6)
	V3	0.14	Good (<0.6)
a_y	V1	0.433m/s^2	Average (0.4~0.5m/s^2)
	V2	0.055m/s^2	Good (<0.4m/s^2)
	V3	0.053m/s^2	Good (<0.4m/s^2)
Roll angle	V1	4.061°	Average (3~5°)
	V2	1.744°	Good (<3°)
	V3	1.357°	Good (<3°)

Specifically, by using an improved artificial potential field algorithm to control the formation, the stability of the following vehicles becomes very good, with the Crt far less than 0.6. Similarly, this algorithm makes the a_y and Roll angle of the following vehicle very small, indicating that the control algorithm has a very significant control effect on the dynamic performance of the following vehicle. When the following vehicle passes through the curve, it is close to equilibrium. It is proved that the vehicle dynamic performance can be obviously optimized by applying the improved artificial potential field algorithm to the dynamic control of formation vehicles.

7. Conclusion

Based on the structure of the new monorail rapid transit vehicle, the dynamic model and multi-body dynamic simulation model of the new monorail rapid transit vehicle are established in this paper. Then the improved artificial potential field algorithm is used to create the formation vehicle operation controller. Then, the dynamic performance evaluation index of the new monorail rapid transit formation vehicle is built, and the formation vehicle passing through the small radius curve scene is simulated. The simulation results show that the dynamic performance of the following vehicle with dynamic control is significantly better than that of the pilot vehicle without control. Crt, a_y and roll angle of the following vehicle can be greatly reduced, which proves the improvement effect of the improved artificial potential field algorithm on the dynamic performance of formation vehicles.

Through the research on the formation operation of

It can be seen from Fig. 10 that the rolling angle of formation vehicles after entering the transition curve increases rapidly, and the maximum rolling angles of formation vehicles are 4.061°, 1.744°, 1.357° respectively. The roll angle of the pilot vehicle is significantly higher than that of the follower vehicle because the pilot vehicle does not control the dynamic performance when passing through the curve. According to the evaluation level of the roll angle in Table 5, the curve passing ability of the pilot vehicle is evaluated as average, and the following vehicle is evaluated as good. It can be clearly seen that the improved artificial potential field controller has the optimization effect on the curve passing ability of formation vehicles. The summary of simulation results is shown in Table 7.

It can be seen from Table 7 that the three evaluation indexes of the following vehicle can reach good, and the values are far lower than those of the pilot vehicle.

new monorail rapid transit vehicles in this article, we believe that urban rail transit vehicles should be able to flexibly operate in formation to adapt to real-time changes in passenger flow. With the saturation of subway line construction, vehicles for small and medium-sized urban rail transit lines in the future should incorporate low-cost and miniaturized design concepts to meet the development and construction needs of various small and medium-sized cities. And new urban rail transit systems will emerge one after another to meet various line needs.

Acknowledgement

References

1. **Haoxin, W.; Zixue, D.; Zhen, Y.;** et al. 2023. Coordination and matching of tire system of new straddle-type rapid transit vehicle, Vehicle System Dynamics 61(2): 573-588.
https://doi.org/10.1080/00423114.2022.2051568.

2. **Zixue, D.; Haoxin, W.; Zhen, Y.;** et al. 2023. Research on Intelligent Formation Operation Performance of Straddle Type Rapid Transit Vehicles in Heterogeneous Operating Environment, Mechanika 29(1): 59-66.
https://doi.org/10.5755/j02.mech.32110.

3. **Junchao, Z.; Zixue, D.; Zhen, Y.** 2019. Dynamic Response of the fullscale Straddle-type Monorail Vehicles with Single-axle Bogies, Mechanika 25(1): 17-24.
http://dx.doi.org/10.5755/j01.mech.25.1.21931.

4. **Junchao, Z.; Zixue, D.; Zhen, Y.;** et al. 2020. Dynamic parameters optimization of straddle-type monorail vehicles based multiobjective collaborative optimization algorithm, Vehicle System Dynamics 58(3): 357-376.
https://doi.org/10.1080/00423114.2019.1578384.

5. **Zixue, D.; Junchao, Z.; Xiaoxia ,W.** 2019. Research of Normal Contact Stiffness of Straddle-Type Monorail Tyres Based on Fractal Theory, Mechanika 25(3): 248-254.
http://dx.doi.org/10.5755/j01.mech.25.3.22265.

6. **Felez, J.; Kim, Y.; & Borrelli, F.** 2019. A model predictive control approach for virtual coupling in railways, IEEE Transactions on Intelligent Transportation Systems 20(7): 2728-2739.
https://doi.org/10.1109/tits.2019.2914910.

7. **Yafei, L.; Ronghui, L.; Congfeng, W.;** et al. 2022. Distributed model predictive control strategy for constrained high-speed virtually coupled train set, IEEE Transactions on Vehicular Technology 71(1): 171-183.
https://doi.org/10.1109/TVT.2021.3130715.

8. **Wang, Q.; Chai, M.; Liu, H.;** et al. 2021. Optimized control of virtual coupling at junctions: A cooperative game-based approach, Actuators 10(9), 207.
https://doi.org/10.3390/act10090207.

9. **Yafei, L.; Yang, Z.; Shuai, S.;** et al. 2021. An analytical optimal control approach for virtually coupled high-speed trains with local and string stability, Transportation research part C emerging technologies 125, 102886.
https://doi.org/10.1016/j.trc.2020.102886.

10. **Shuai, S.; Wentao, L.; Qingyang, Z.;** et al. 2022. A cooperative collision avoidance control methodology for virtual coupling trains[J], Accident Analysis & Prevention 173, 106703.
https://doi.org/10.1016/j.aap.2022.106703.

11. **Di Meo, C.; Di Vaio, M.; Flammini, F.;** et al. 2020. ERTMS/ETCS virtual coupling: Proof of concept and numerical analysis, IEEE Transactions on Intelligent Transportation Systems. 21(6): 2545-2556.
https://doi.org/10.1109/TITS.2019.2920290.

12. Mechanical vibration-Road surface profiles-Reporting of measured data. ISO 8608-2016. International Organization for Standardization, 2016.

13. **Haowei, Y.; Yi, X.; Junyu, K.;** et al. 2019. Study on the Standard Value of Passenger Comfort Control for Suspended Monorail Planar Circular Curve, Rail-way standard design 63(7): 57-61.
https://doi.org/10.13238/j.issn.1004-954.201808250004.

H. Wu, Z. Du, Z. Yang, X. Wen

DYNAMIC PERFOMANCE OPTIMIZATION OF MONORAIL RAPID TRANSIT FORMATION VEHICLES BASED ON IMPROVED ARTIFICIAL POTENTIAL FIELD ALGORITHM

S u m m a r y

This paper presents a new type of monorail rapid transit vehicle, which can operate in formation. In order to optimize the dynamic performance of the formation vehicles when passing through the small radius curve, this paper first analyzes the structure of the new monorail rapid transit vehicle, and establishes the vehicle dynamic model and multibody dynamics simulation model. Then the improved artificial potential field algorithm is used to build the formation vehicle operation controller. Finally, the dynamic performance evaluation index of the new monorail rapid transit formation vehicle is formulated, and the formation vehicle passing through the small radius curve scene is simulated. The simulation results show that the controller of the formation vehicle with dynamic optimization control can effectively optimize the load transfer coefficient of running wheels, unbalanced centrifugal acceleration and roll angle of vehicle body when passing through the curve. Through this control method, the dynamic performance of formation vehicles passing through small radius curve lines can be optimized.